Macromolecules

Article

pubs.acs.org/Macromolecules

Network Structure and Inhomogeneities of Model and Commercial Polyelectrolyte Hydrogels as Investigated by Low-Field Proton NMR Techniques

Johannes Höpfner,[†] Gisela Guthausen,[†] Kay Saalwächter,*[,‡] and Manfred Wilhelm*[,†]

[†]Institute for Chemical Technology and Polymer Chemistry, Karlsruhe Institute of Technology (KIT), Karlsruhe, Germany

[‡]Institut für Physik—NMR, Martin Luther Universität Halle-Wittenberg, Halle (Saale), Germany

Supporting Information

ABSTRACT: This work presents an experimental study of the network structure of swollen, charged hydrogels. We provide an in-depth comparison of two proton low-field NMR methods, i.e., transverse relaxation and double-quantum spectroscopy, that are both sensitive to residual orientation correlations of the network chain segments. The results are in both cases analyzed by help of integral inversion techniques, and both methods are demonstrated to provide comparable results despite the more qualitative nature of the transverse relaxation. We investigate model samples that are similar to commercial superabsorber materials based on partly neutralized and chemically cross-linked poly(acrylic acid) as prepared by free radical polymerization. The degree of cross-linking and the monomer concentration are varied during synthesis. Both parameters are found to affect the network structure and the amount of elastically inactive defects in a systematic way, and a comparison with commercial samples with homogeneous or purposely inhomogeneous core−shell structures proves that the cross-linking bimodality of the latter is readily revealed despite the rather large intrinsic inhomogeneity of the swollen gels.

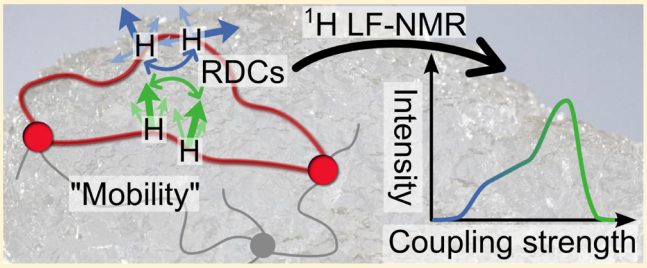

INTRODUCTION

Polymeric hydrogels have been the subject of intensive investigation over the past years.[1−6] The current focus is on the development of hydrogels that are responsive to one or more stimuli[1,2] or the preparation of super tough gels with high moduli and high elongations at break.[3,4] This interest in gels is stimulated by the many current and proposed technical applications including drug delivery,[5] sensors and actuators.[6] In addition, we recently proposed for the first time, the use of gels as separation material for water and ions, with seawater desalination as an important potential application.[7−9]

Hydrogels are polymeric materials composed of covalently cross-linked chains. These networks have a very large swelling capability due to the hydrophilic nature of the monomers, which is augmented by charges bound to the strands (so-called polyelectrolytes).[10] The mesh size in the network is the most important factor in controlling the gels properties. However, only a few examples of gels with a rather well-defined mesh size are known.[11,12] Typically, the mesh size is not well-defined nor uniform but set by the statistical copolymerization process that leads to the gel's formation.[13] This distribution of chain length between two nodes and the imperfections such as dangling ends and highly cross-linked domains lead to very inhomogeneous structures.

Despite the numerous investigations, the structural inhomogeneities of networks, especially on the mesoscale, are not well understood.[12,14] However, they may exert a strong influence on gel properties such as mechanical strength, swelling capacity,[14] and ion uptake or rejection. Previous structural characterization of the polymeric network in swollen gels included scattering techniques e.g. SLS, DLS, SANS, or various NMR techniques.[4,12,14−26] These studies revealed that the swollen state is particularly characterized by so-called swelling inhomogeneities arising from the unfolding of a topologically complex structure, implying a strong dependence on the preparation conditions of the gel and the degree of swelling.

The structure of networks is known to be reflected in the mobilities of network chains which can be accessed using NMR relaxometry and related methods like double quantum (DQ) spectroscopy.[27] In particular, proton NMR experiments that can be performed at low fields (LF-NMR), were proven to provide versatile tools in the quantitative characterization of molecular dynamics and structure of polymer networks (for examples see, e.g., refs 28−31). The theoretical underpinning of the relationship between mobility and NMR observables is discussed in the following section.

LF-NMR methods were successfully used on polymeric networks such as rubbers. For example, a comparison of experiments on bulk and swollen rubbers can provide information on entanglement contributions to rubber elasti-

Received: March 17, 2014
Revised: June 4, 2014
Published: June 25, 2014

   dx.doi.org/10.1021/ma500558v | Macromolecules 2014, 47, 4251−4265

city,[32] and studies at variable degrees of swelling have revealed the complex topological unfolding processes.[33] Additionally, the above-mentioned imperfections are accessible by LF-NMR.[31,34]

In contrast to rubbers, systematic and quantitative NMR-relaxation studies on hydrogels are scarce, especially concerning industrially relevant systems such as poly(acrylic acid) which is the basis of superabsorbers (e.g., in diapers). Most LF-NMR studies on hydrogels focus on more qualitative analyses in the areas of food science[35] or pharmaceutical technology.[36] In particular, the relation of spatial inhomogeneities of the cross-links to macroscopic properties (e.g., mechanical), has rarely been studied in a systematic fashion.[37] On the other hand, it is known from independent studies that both properties are strongly dependent on the preparation conditions, in particular the cross-linking chemistry.[34,38] Simulations indicate that in swollen samples load transmission and chain stretching are dominated by strong structural inhomogeneities.[39]

The main motivation for the present work is to demonstrate for the first time a comprehensive characterization of polyelectrolyte network structure and dynamics by the most promising low-field NMR techniques, arriving at structural information that cannot easily be obtained by alternative techniques. In this article, we highlight how changes in network structure and dynamics can be discovered using time-domain correlations in gels while systematically varying the gel composition. We specifically use LF-NMR at 0.47 T ($\omega_0/2\pi$ = 19.95 MHz), which does not represent a disadvantage at all since the resonance lines in the investigated cross-linked polyelectrolyte are broadened anyway, an effect commonly found for cross-linked polymers.[40] As will become apparent, the acquired time-domain signals faithfully reflect the overall mobility in the samples.[41,42] It is important to note that the DQ method in particular is also applicable at low field and was, to our knowledge, only applied to uncharged gels up to now.[12,19] Therefore, this study is exploring the possibilities to use this method in charged gels and intends to give guidelines for the proper application of LF-NMR methods to cross-linked polyelectrolyte samples.

THEORETICAL PRINCIPLES OF PROTON T_2 AND DQ NMR EXPERIMENTS

The molecular dynamics of polymer chain segments in a network as probed by NMR can be directly connected to the network structure. In short, the main effect arises from the orientation-dependent homonuclear dipolar couplings of neighboring spins (mostly protons) along the chain, which means all relevant NMR observables can be related to the orientation autocorrelation function (OACF) of chain segments as the most relevant descriptor of the molecular dynamics.[43] In networks, the segmental OACF does not decay to zero but exhibits a long-time plateau which arises from the network constraints (cross-links). The degree of residual correlation, and thus the degree of cross-linking, can be probed by either recording and analyzing transverse relaxation decays, or by a more direct analysis of residual dipolar couplings (RDCs). Both analysis methods are employed and compared below.

In quantitative terms, the transverse ^{1}H relaxation rate depends mainly on the coupling of neighboring spins, which is described by the homonuclear dipolar Hamiltonian $\hat{H}_d$ as a function of the internuclear distance r and the orientation Θ of two protons relative to the applied magnetic B_0 field by

$$\hat{H}_d = \frac{\mu_0 \gamma^2 \hbar^2}{4\pi r^3}(3\cos^2\Theta - 1)(3\hat{I}_{1,z}\hat{I}_{2,z} - \hat{I}_1\hat{I}_2) \quad (1)$$

where $\hat{I}_i$ are the spin operators of the coupled protons. The dipolar interaction between neighboring spins is modulated by molecular motion leading to a relaxation path for nuclear magnetization that is usually modeled by the OACF. The spectral density function $J(\omega, \tau_c)$ is connected with the OACF by a Fourier transformation (FT). According to the theory of Bloembergen, Purcell, and Pound (BPP), $J(\omega, \tau_c)$ determines the NMR relaxation rates R_i.[44] For example, the transverse relaxation time T_2 obeys for two coupled protons[45] the modified formula

$$\frac{1}{T_2} = R_2 = \frac{3\gamma^4\hbar^2}{40\langle r\rangle^6}[3J(\Delta\omega) + 5J(\omega_0) + 2J(2\omega_0)] \quad (2)$$

where γ is the magnetogyric ratio of the spins, $\langle r\rangle$ is their average distance and ω_0 is the Larmor angular frequency. T_2 relaxation is of particular interest for the investigation of cross-linked systems, as it is sensitive to the rather slow motions on the time scale of the inverse dipolar line width for $T \to 0$ ($\Delta\omega$). They are related to cooperative chain dynamics and is influenced by constraints such as cross-link points. It is possible to calculate the relaxation rates from $J(\omega, \tau_c)$ by assuming an appropriate model for the OACF. However, simple models that can be solved analytically, such as rotational diffusion in an isotropic liquid lead to a single exponential OACF that decays to zero on a correlation time scale below the one observed in NMR experiments (milliseconds to microseconds). Therefore, these models are not sufficient for networks and hydrogels. This is due to the longer time scales of the multiexponential chain relaxations, network heterogeneity, and in particular to the mentioned residual anisotropy.

While a general expectation of faster T_2 relaxation in less mobile samples can be formulated, the major conceptual problem of the BPP-based approach is that it does not account for a decisively nonexponential T_2 decay, which is ultimately related to the residual temporal and spacial anisotropy. Therefore, the overall T_2 time scale is qualitatively reflected in the dominating $J(\Delta\omega)$ term. A proper intermediate-motional theory such as the Anderson–Weiss ansatz is needed to derive the exact shape of the relaxation function.[27] This ansatz is sensitively dependent on the shape of the OACF and care has to be taken when predicting it.[46]

However, in rubbers far above the glass transition, and thus also in hydrogels, where only the long-time plateau value (the residual anisotropy) matters, the proton transverse relaxation can be described by a Gaussian-shaped dipolar dephasing function,[27,43,46]

$$I(t_{echo}) = A\exp\left\{-\frac{9}{40}D_{res}{}^2 t_{echo}{}^2\right\} \quad (3)$$

D_{res} is directly proportional to the square-root of the long-time plateau value of the normalized OACF, which is termed the dynamic chain order parameter S_b

$$D_{res} \propto S_b \approx \frac{3r^2}{5N_c} \quad (4)$$

where N_c is the number of statistical segments per network mesh and $r = R/R_0$ is the ratio of the end-to-end distance of the network chain to its average unperturbed value.[17,43] D_{res} thus reflects the structure as well as a potential, swelling-induced

dx.doi.org/10.1021/ma500558v | Macromolecules 2014, 47, 4251–4265

Scheme 1. Schematic of the Synthetic Procedure for the Preparation of the Studied Model Hydrogels[a]

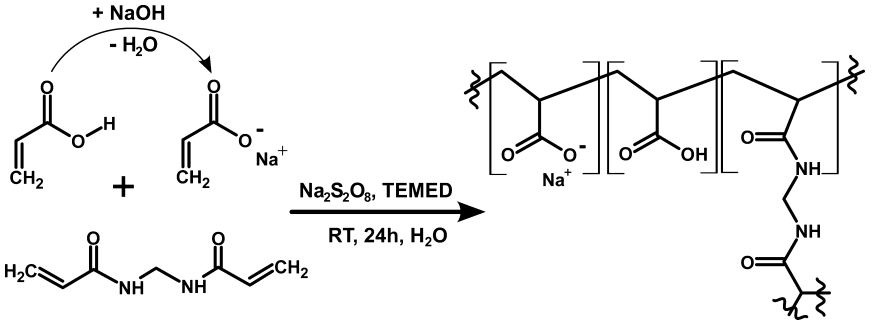

[a]The gels were prepared by free radical polymerization initiated by a redox system of sodium persulfate (SPS, $Na_2S_2O_8$) and *N,N,N′,N′*-tetramethylethylenediamine (TEMED) at room temperature. Acrylic acid was partly neutralized (typically 78 mol %) by sodium hydroxide and the tetrafunctional cross-linker *N,N′*-methylenebis(acrylamide) was copolymerized. Parts of the resulting gel structure are shown on the right.

deformation of the network chains. Now, instead of relying on ambiguities related to the shape of the transverse relaxation decay, the residual dipolar coupling can directly and reliably be measured by using double-quantum (DQ) experiments.[43,47] DQ spectroscopy in its most robust form involves the measurement of an intensity build-up function which is only dependent on D_{res}.[43] Therefore, DQ spectroscopy employs a normalization procedure to remove any incoherent contributions arising from the time scale of chain fluctuations. In case of T_2 relaxation, this can lead to a partially exponential character on top of its Gaussian shape. Within the same type of second-moment approximation that leads to eq 3, a generic DQ build-up function can be derived, which reads

$$I(t_{DQ}) = \frac{1}{2}\left[1 - \exp\left(-\frac{2}{5}D_{res}^{2}t_{DQ}^{2}\right)\right] \quad (5)$$

Again, actual data exhibits deviations from such an inverse Gaussian shape, which is on the one hand due to some quantum-mechanical intricacies[48] that can be accounted for and are not very relevant in the present context, and on the other hand, importantly, due to network inhomogeneities. I.e., a real-life sample with segments (monomers) in different environments is not described by a single D_{res}.

A fundamental problem of each measurement technique in polymeric networks is thus to choose appropriate representation techniques for the structural and dynamic heterogeneity of the cross-linked systems. Both methods, transverse relaxation and DQ spectroscopy, are capable of measuring the heterogeneity in dynamics as part of the composite signal. However, the deconvolution and resolution of a continuous distribution into potentially distinct components remains a challenge. Empirical fit functions were often used to describe transverse relaxation data, such as combinations of regular or stretched exponential functions or Gaussian functions (e.g. refs 30, 49, and 50). However, the unambiguous assignment of the time constants to specific processes is difficult.

A promising alternative to the use of fit functions are integral transformation methods. As a results of such transformations the distributions of the underlying parameters (decay time or RDC constants) are obtained. A widely used method for the integral transformation of relaxation data is the inverse Laplace transform (ILT). In this work we use the implementation of Callaghan et al.[51,52] Unfortunately, due to theoretical considerations the ILT is limited to analyze relaxation data that is produced by purely exponential processes[53,54] but often nonexponential (in particular Gaussian-shaped) decays contribute as well. It has therefore often been argued that the ILT should not be used in such cases. We would like to contradict this by stating the ILT can obtain qualitatively meaningful results when analyzing broadly distributed Gaussian-based decays as well. We support this by a test case shown at the end of this article. For the analysis of the double quantum data the more general approach of Tikhonov is used. It allows to use various kernel functions including an inverted Gaussian. Recently, Chassé et al. introduced a more advanced kernel function for the analysis of RDC distributions,[48] which we employ here. It should also be noted that such integral transformations of noisy data based upon monotonic Kernel functions belong to the class of mathematically ill-posed problems. A regularization or error parameter must be monitored to ensure meaningful results.[48]

EXPERIMENTAL DETAILS

Reagents and Purification. The hydrogel samples were prepared using the following chemicals. Acrylic acid (AAc, 99%, stabilized, Sigma-Aldrich, Germany) was distilled at 23 mbar with a boiling point of 43 °C prior to use. *N,N′*-Methylenebis(acrylamide) (MBA, 99+ %), aqueous sodium hydroxide solution (33 wt %, extra pure), sodium peroxodisulfate (SPS, 98+ %), and *N,N,N′,N′*-tetramethylethylenediamine (TEMED, 99%) were all obtained from Acros, Belgium, and used as received. Deuterated water (D_2O, 99.97% deuterated) for swelling the samples prior to NMR measurements was obtained from euriso-top, France, and used as received.

Hydrogel Preparation. The model gels used in this study were prepared by free radical cross-linking polymerization to have control over the sample composition or obtained from an industrial source for comparison. The latter samples were Luquasorb batches 1030 and B1110 (BASF, Germany) designated herein as L1030 and LB1110. The synthetic approach was adapted from known procedures[55−57] and is depicted in Scheme 1. A typical batch consisted of 1.16 g of the cross-linker MBA (0.01 eq, 7.5 mmol), which was dissolved in 215 mL of deionized water and 54 g of AAc (1 equiv, 0.75 mol) were added. The mixture was cooled in an ice bath to $T \approx 5$ °C. While stirring, the mixture was partly neutralized by adding dropwise 50.1 mL (0.75 equiv) sodium hydroxide solution. A dropwise addition was necessary as the temperature should not exceed 12 °C to prevent premature polymerization. Next, 360 mg SPS (0.002 equiv, 1.5 mmol) were dissolved in 2 mL of deionized water and added to the AAc solution. The solution was further cooled and purged for 30 min with nitrogen gas to remove residual oxygen. The reaction was started by removing the cooling bath and adding 1.74 g of TEMED (0.02 equiv, 15 mmol). Within some minutes at room temperature, the gel point was reached. The reaction was left to proceed for another 12 h after which the resulting clear, colorless gel was cut, dried in vacuo at 70 °C, and

dx.doi.org/10.1021/ma500558v | Macromolecules 2014, 47, 4251−4265

ground with a rotary mill (cooled to 100 °C) to a dry bead diameter of less than 0.6 mm.

Hydrogels with different properties and molecular structures can be obtained by changing the composition of the synthesis mixture. Three parameters were used to influence the structure and mobility: the degree of cross-linking (DC, eq 6), the degree of neutralization (DN, eq 7) and the water content of the synthesis mixture (Q_{syn}, eq 8). These parameters are defined with respect to the amount of AAc in the mixture.

$$\mathrm{DC\ [mol\ \%]} = \frac{n(\mathrm{MBA})}{n(\mathrm{AAc})} \times 100\% \tag{6}$$

$$\mathrm{DN\ [mol\ \%]} = \frac{n(\mathrm{NaOH})}{n(\mathrm{AAc})} \times 100\% \tag{7}$$

$$Q_{syn}\ \mathrm{[g/g]} = \frac{m(\mathrm{H_2O})}{m(\mathrm{AAc}) + m(\mathrm{MBA})} \tag{8}$$

Using this procedure a number of gels were synthesized by varying in four steps DC (0.1−3.1 mol %) or Q_{syn} (1.6−8 g/g) each to cover a broad range of possible compositions, while DN was between 75−85 mol % for all samples as this resulted in the maximal swelling capacity. The respective compositions of the investigated samples are listed in Table 1.

Table 1. List of Model Hydrogel Samples Synthesised for This Work[a]

sample	DC [mol %]	Q_{syn} [g/g]	DN [mol %]
pAAc-DC0.1-Q4	0.1	4	76
pAAc-DC0.3-Q4	0.3	4	83
pAAc-DC1-Q4	1	4	76
pAAc-DC3-Q4	3.1	4	85
pAAc-DC1-Q1.6	1	1.6	76
pAAc-DC1-Q2	1	2	75
pAAc-DC1-Q8	1	8	75

[a]The values for the synthesis parameters, as defined in eqs 6−8, are summarized. In the sample designation, the first number gives the degree of cross-linking (in mol %) and the second the water content at the time of synthesis (in g of water per g of polymer).

Swelling Capacity and Sol Content. The samples were characterized by their equilibrium swelling capacity and the content of extractable polymeric material (sol). The swelling capacity Q_{eq} is the amount of solvent a gel takes up in its equilibrium state and is determined gravimetrically.[58] The dry polymer with mass m(PM) was placed on a sieve (m(sieve)). Typically, 20 to 100 mg of dry polymer beads were used where the selected amount increased with the expected degree of swelling. The sieve was then lowered to be in contact with an excess of deionized water (at least 20 times the final water uptake). The hydrogel was left to swell for at least 24 h at room temperature and sealed to prevent evaporation. After swelling, the sieve was gently pressed on a sheet of paper towel for 30 s to remove excess solution and then weighed to obtain m(wet). The swelling degree is calculated by eq 9. The average of three measurements was taken for each sample and the difference between the largest and the smallest value was typically below 2%.

$$Q_{eq} = \frac{m(\mathrm{H_2O})}{m(\mathrm{PM})} = \frac{m(\mathrm{wet}) - m(\mathrm{sieve}) - m(\mathrm{PM})}{m(\mathrm{PM})} \tag{9}$$

The sol content of a hydrogel sample was determined by mixing 0.5 g of the dry polymer (m(PM)) with deionized water (m(water)). The mass ratio of water to gel was more than 5:1 with respect to the final volume of the gel. The mixture was sealed and stirred for 2 weeks at room temperature. Then, the mixture was filtered through a 5 μm pore size filter paper and the filtrate was weighed to give m(filtrate). Next, the water was evaporated using in a rotary evaporator followed by drying in vacuo at 70 °C and the sol content was obtained from the mass of residue m(sol). Assuming an equipartition of the sol in gel and the solution phases, the sol fraction can be calculated by eq 10. For measurement of sol free gels in the NMR experiments, the residual gel in the filter was dried again and prepared as mentioned before.

$$\mathrm{sol\ content\ [wt\ \%]} = \frac{m(\mathrm{sol})\frac{m(\mathrm{DI})}{m(\mathrm{filtrate})}}{m(\mathrm{PM})} 100\% \tag{10}$$

The average of three measurements was taken as well, and the difference between the largest and the smallest value was typically within 20%.

NMR Instrument and Measurements. The low-field NMR measurements were carried out on a benchtop minispec mq20 (Bruker, Germany). It uses a permanent magnet to create a field (0.469 T) corresponding to a proton resonance frequency of 19.95 MHz. The sample temperature was independently controlled by a BVT3000 (Bruker Variable Temperature Unit) using a temperature-conditioned air flow and was kept between 30−32 °C. For all samples the magnetic field was matched to the resonance circuit, and the duration of the broad-band $\pi/2$- and π-pulses were determined individually by a nutation experiment. The durations were in the order of 2.7 and 5.1 μs at full amplitude for $\pi/2$- and π-pulses, respectively. On resonance experiments resulted in FID half-lives of 2 ms or longer after a $\pi/2$-pulse as a result of dipolar coupling and field inhomogeneities. The samples for NMR measurements were prepared from the polymers described above. About 60 mg of dried polymer particles were mixed with D_2O in a ratio of 1:9 by weight on a glass plate. The polymer was subsequently dried in vacuo at 70 °C and then mixed again with the same ratio of D_2O, to reduce the proton content from residual H_2O. After the second swelling, the resulting gel was transferred to the bottom of a NMR glass tube with 10 mm outer diameter. The tube was stoppered and sealed with Parafilm to prevent evaporation and left to equilibrate for at least 24 h before the measurements. The filling level and placing of the sample in the magnet must be adjusted to bring the whole sample into the region of the highest homogeneity of the magnet fields B_0 and B_1. Usually, the sample height did not exceed 8 mm.

The spin−spin relaxation behavior of the gels was recorded using the magic sandwich echo (MSE),[27,59,60] CPMG,[61,62] and Hahn-echo[63] pulse sequences. The acquisition parameters of the experiments are listed in Table 2. The program for measuring the MSE was implemented from literature.[27,60] The CPMG and Hahn echo sequences were part of the standard programs provided by Bruker (t2_cp_mb.app and t2_se_mb.app, respectively). However, it was necessary to modify the phase cycle of the -pulse train of the CPMG pulse sequence, as described in the Results, to make it suitable for this

Table 2. Measurement Parameters Used in the NMR Experiments To Determine the Transverse Relaxation Behavior (T_2) and the Residual Dipolar Coupling Strength[a]

	CPMG/XY16					
pulse sequence	short delay	medium delay	long delay	Hahn echo	MSE	DQ
ns [−]	256	128	128	48	128	1024
ds [−]	4	4	4	4	4	16
τ_E [ms]	0.04	1	1	0.04−100	—	—
de [−]	0	0	15	0	—	—
rd [s]	20	20	20	20	20	0.1
ne [−]	256	256	256	1	—	—

[a]The parameters are the number of acquired scans (ns), the number of non-acquired dummy scans (ds), echo time (τ_E), the number of non-acquired echoes (de) per acquired echo, recycle delay (rd), and the number of acquired echoes (ne). For further explanation of the experiments please see the text.

dx.doi.org/10.1021/ma500558v | Macromolecules 2014, 47, 4251−4265

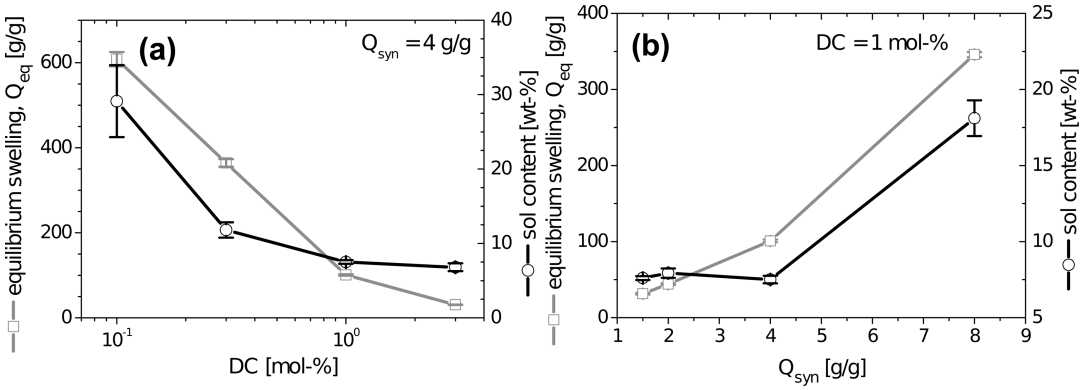

Figure 1. Equilibrium swelling capacity in deionized water and the sol content are shown for two series of model hydrogel samples synthesized by free radical polymerization. The degree of cross-linking (DC) was varied (a) while the water content at the time of synthesis was fixed at Q_{syn} =4 g/g. In part b, samples with varying values of Q_{syn} at a fixed value of DC = 1 mol % are shown. For all samples, the degree of neutralization of acrylic acid was similar in the range of 75−86 mol %. The lines are guides to the eye.

investigation. The XY16-phase cycle[64] was implemented into the CPMG program (see the Supporting Information for phase cycles). The standard CYCLOPS phase cycle[65] is superimposed on the XY16 scheme to compensate for instrumental errors.

The transverse relaxation processes in the investigated samples spanned a large time scale up to 6 decades. As it was not possible to acquire the complete decay with a single experiment, a composite approach was used. The fastest part of the decay was probed by the first 100 μs of the FID using the MSE. The later part was recorded by three CPMG/XY16 experiments by increasing the echo time τ_E and by introducing nonacquired echoes (de) as given in Table 2. The results from all four experiments was collected into a single data set, the solvent signal was then subtracted, and the data was normalized (see Supporting Information).

The DQ-experiments were performed by a pulse sequence disclosed in earlier publications.[43,48] The acquisition parameters were tuned for optimal signal quality for hydrogel samples. In these experiments, 70 points of data were recorded for the DQ and reference intensity with an initial spacing of 0.04 ms, which was doubled after each 10 points (see also Table 2).

RESULTS AND DISCUSSION

Swelling Capacity and Sol Content. Important quantities which characterize polymeric networks are the equilibrium swelling capacity, Q_{eq}, and the sol content. The former is measured by the weight of water uptake in deionized water and the latter by the weight of nonvolatile compounds that pass into the surrounding solution phase. These parameters were measured for samples of increasing cross-link density DC at fixed Q_{syn} = 4 g/g and then for samples with increasing water content at the time of synthesis Q_{syn} at fixed DC = 1 mol %. The results are given in Figure 1. For the commercial samples, swelling capacities of 106 and 215 g/g and sol contents of 4.4 and 14.2 wt % were measured for LB1110 and L1030, respectively.

The results show a strong decrease in the swelling capacity and sol content with an increase of DC. This is a consequence of the higher number of nodal points in the network as the shorter meshes can be extended less during swelling. Additionally, the probability of incorporating at least one cross-linker molecule into a growing polymer chain increases with an increasing DC consequently lowering the sol content. In a similar fashion, for a higher monomer concentration at the time of synthesis (low Q_{syn}), a denser network is formed. This causes the network to be strongly interdispersed with additional cross-links from trapped entanglements. This also reduces the swelling capacity. In contrast, a higher dilution of the monomer during synthesis favors the formation of defects such as dangling ends and sol chains. However, a small part, about 8 wt %, of sol is present for all model samples. This effect has been observed before[66,67] and might indicate the presence of inherent imperfections inherent to the synthesis method, e.g., early chain termination or a very broad distribution of chain length.

Measurement of the Unbiased Magnetization Relaxation Behavior. As a first experiment, the longitudinal proton relaxation in the laboratory frame (T_1) was investigated and found to be almost independent of the hydrogel composition. By a saturation recovery experiment, a double exponential relaxation with time constants on the order of seconds (HDO) and around 30 ms (polymer component) were found. The results were almost unaffected by chemical changes of the samples (not shown). The longitudinal relaxation probes high frequency motions in the range of many MHz, which are mostly unaffected by the weak constraints posed by the cross-linking of the chains. Therefore, the longitudinal relaxation was not investigated further.

In contrast, the recording of the transverse relaxation of magnetization probes much slower motions that are strongly affected by the network structure. Yet, their measurement was only successful when the unique properties of the sample and instrument were recognized and appropriate methods were used. In LF-NMR, the transverse magnetization decay cannot be obtained directly from the free induction decay (FID) due to its shortening by field inhomogeneities. Therefore, the magnetization has to be recovered by spin echo techniques (e.g., Hahn echo or CPMG). The magnetization decays are measured as a function of the echo time τ_E (Hahn echo) or the number of echoes $n \times \tau_E$ (CPMG). Usually, the CPMG experiment is preferred as it is able to capture several points of the decay within one experiment. However, when the relaxation curve spans a very large time scale, it cannot be covered by one CPMG echo train (even with a very high number of echoes). Instead, the delay in between echoes τ_E must be increased. As the same relaxation process is investigated, the results of Hahn and CPMG echo experiments with different delays are expected to coincide on the same decay curve as long as the pulse spacing is shorter than the system's dynamics.

However, when the results of the two methods applied to a typical hydrogel sample are compared (Figure 2a), this was not

dx.doi.org/10.1021/ma500558v | Macromolecules 2014, 47, 4251−4265

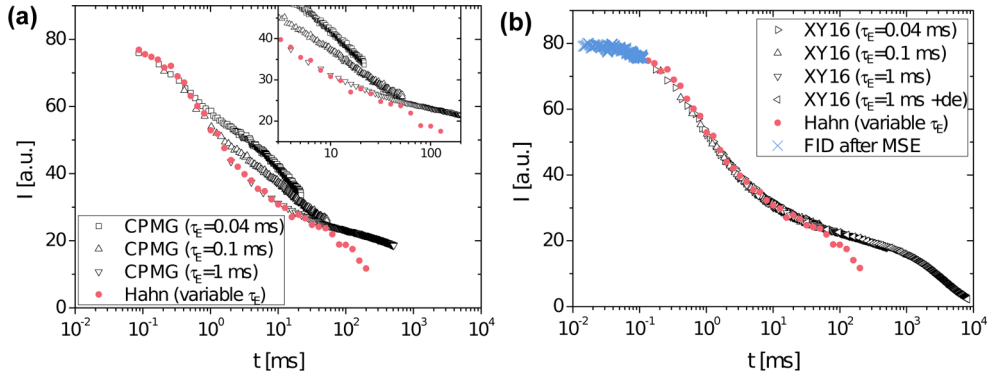

Figure 2. Decay of the transverse magnetization in a typical hydrogel is shown (DC = 1 mol %, Q_{syn} = 4 g/g). It is measured by a CPMG echo train and Hahn echo experiments with different values for the separation of π-pulses (τ_E). The standard CPMG sequence (a) is compared to a multiecho sequence with XY16 phase cycling (b) with use of nonacquired echoes (de). Avoiding $T_{1\rho}$ spin lock effects using the XY16 sequence, the multiecho decay is independent of τ_E. In part b, additionally, the decay measured from the FID after a magic sandwich echo is shown.

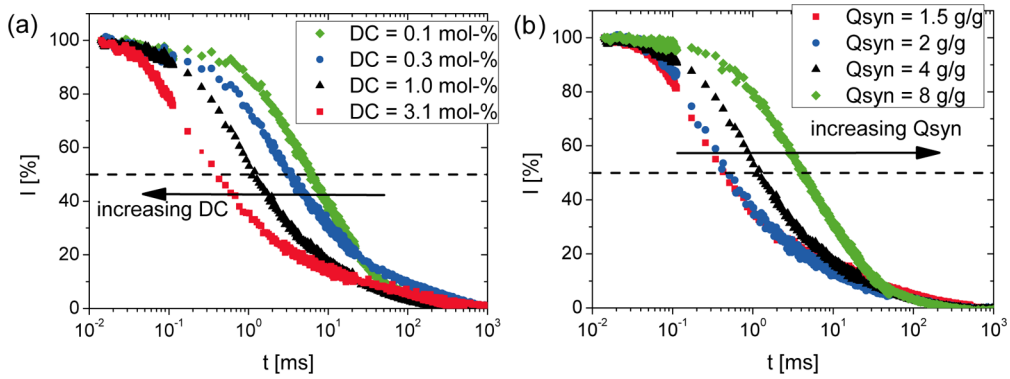

Figure 3. Normalized decay of the transverse magnetization is shown for model hydrogels of various compositions in their as prepared state. A series of samples with an increasing degree of cross-linking (DC) is investigated (a) at constant Q_{syn} = 4 g/g and the monomer concentration at the time of synthesis is changed (b) at constant DC = 1 mol %. The dashed line indicates the half-life of the magnetization.

the case: with increasing pulse separation τ_E for the CPMG experiments (open symbols), the relaxation apparently becomes faster. When shown together, only the first few data points of each CPMG data set overlap with the results from the Hahn echo experiment (solid dots). The apparent relaxation process takes place on different time scales in each measurement. The reason for this peculiar result can be found in the spin-lock effect of the applied NMR pulses.[68,69] The close spacing of the pulses with identical phase at short τ_E values in the CPMG-echo train mimics a locking field. Such a field is used to measure the longitudinal relaxation in the rotating frame ($T_{1\rho}$).[68] The magnetization decays in the rotating frame in accordance with $T_{1\rho}$, which for the investigated samples is longer than T_2 and leads to a slower apparent relaxation. For long τ_E, the difference decreases and the CPMG trace coincides with the Hahn echo data, which are not affected by the spin lock effect. Yet, the decay from the Hahn echo method decays faster than the "true" spin−spin-relaxation of the system for large pulse spacings. The refocusing of magnetization when τ_E is longer than 50 ms is probably hampered by slow time variations of the B_0 field of our spectrometer.

To avoid spin-lock effects in CPMG experiments the pulse phases within the echo train are cycled to prevent averaging of the B_1 field to a nonzero effective field B_{1eff}. Advanced phase cycling schemes such as XX4 (also called MLEV-4)[70] and XY16[64,69] are known and were tested. Only the latter scheme produced satisfactory results and all measurements coincide on one curve as shown in Figure 2b.

The transverse magnetization decay was observed over 6 orders of magnitude in time and had to be recorded by several measurements. The fast initial decay was probed by the (nonincremented) magic sandwich echo (MSE), which would otherwise be lost due to the dead time (about 14 μs in this case). The MSE is an improved version of the solid echo.[59,60] The later decay is acquired by CPMG/XY16 with a short echo time compared to the diffusion time in the sample (see above). By these measures, the unbiased transverse relaxation of the samples can be measured and evaluated in a meaningful way.

Transverse Relaxation as a Function of Gel Composition. The decay of the transverse magnetization was obtained for model hydrogel samples produced with various compositions as described above. From the magnetization decay, the mono exponential solvent signal (HDO) was subtracted ($T_2 \approx$ 3 s) and the data was normalized to 100% at the first point (see Supporting Information for details). The resulting curves are shown in Figure 3 as a function of the degree of cross-linking (DC) and the water content at the time of synthesis (Q_{syn}).

For both sample series, a clear dynamic contrast was found between the samples. The half-life times of the signals (dashed line) changed by more than 1 order of magnitude within the investigated range of compositions. The observed trends correlated with the synthesis variables: larger DC lead to faster decay, and higher Q_{syn} caused slower decay of the magnetization. As mentioned in the introduction, more constraints in the hydrogel reduce the overall mobility and speed up the relaxation process and shorten (T_2). This increase in molecular

dx.doi.org/10.1021/ma500558v | Macromolecules 2014, 47, 4251−4265

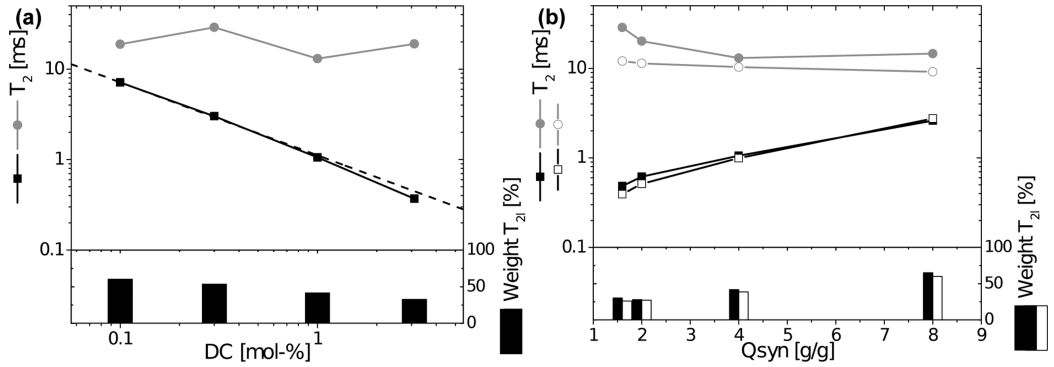

Figure 4. Time constants $T_{2,s}$ (black) and $T_{2,l}$ (grey) were obtained by applying the fit function given by eq 11 to the transverse relaxation data shown in Figure 3. A series of samples with increasing degree of cross-linking (DC, with constant Q_{syn} = 4 g/g) was investigated (a) and the monomer concentration at the time of synthesis (Q_{syn}, at constant DC = 1 mol %) was changed (b). The filled symbols/bars represent as prepared samples and open symbols/bars samples from which the sol has been removed. The solid lines are a guide for the eye while the dashed line in part a is a power law fit with an exponent of −0.81. The bars represent the weight of the component with the longer time constant.

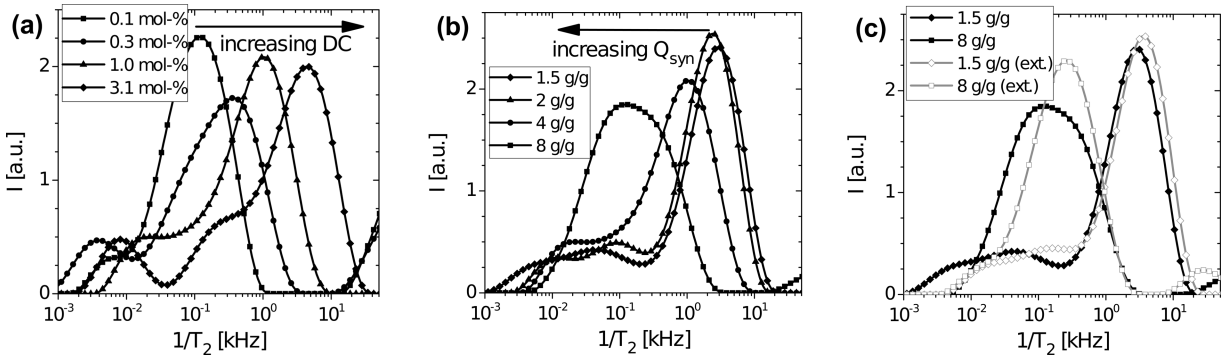

Figure 5. Distributions of T_2^{-1} obtained by the inverse Laplace transform of the data in Figure 3 are shown for the as-prepared samples. A series of samples with increasing degree of cross-linking (DC) is shown (with constant Q_{syn} = 4 g/g) in part a and the monomer concentration at the time of synthesis (Q_{syn}) varies in part b (at constant DC = 1 mol %). The data sets with the highest and lowest Q_{syn} from part b are replotted in part c with the corresponding data sets where the sol has been extracted (gray lines).

constraints can be accomplished by either a higher cross-link density or a more concentrated polymerization mixture (lower Q_{syn}), which leads to strongly interdispersed and entangled meshes. Also, the probability of mobile defects such as sol and dangling ends is reduced. It should be noted that for the samples with the fastest decay (highest DC), simple echo experiments would not have been sufficient as up to 30% of the signal decays before the first point of the CPMG echo train is recorded. This can be circumvented by the use of the MSE.

Evaluation of Relaxation Data. The obtained relaxation data can be analyzed by the two previously mentioned approaches. Specifically, the use of an empirical fit function or an inversion procedure of the time dependent data can be applied. Several empirical two component fit functions were examined to find a good representation of the data with a minimal number of degrees of freedom. The best result was obtained for the combination of an exponential with a stretched exponential function (also called KWW-function) as given by eq 11, where A is the relative weight of the single exponential and $\beta < 1$ the stretching parameter.

$$I(t) = A \exp\left(-\frac{t}{T_{2,s}}\right) + (100 - A) \exp\left(-\left(\frac{t}{T_{2,l}}\right)^{\beta}\right) \quad (11)$$

The obtained fit parameters are the data in Figure 3 are given in Figure 4 and are listed in the Supporting Information as well.

The time constants obtained from the fits follow the same clear trend observed for the raw data. Specifically, the shorter time constant $T_{2,s}$ is decreasing for an increase in DC and a decrease in Q_{syn}. In contrast, the larger time constant, $T_{2,l}$, is almost unaffected by changes in the gel synthesis. The weight of $T_{2,s}$ follows this trend and increases monotonically. The dependence of $T_{2,s}$ is almost linear with the logarithm of DC and is well described by a power law with an exponent of −0.81 (prefactor 1.1, shown as the dashed line in Figure 4). The parameter β is in the range of 0.4−0.7.

Additionally, for the samples with varying values of Q_{syn} at constant DC, the sol was extracted and the remaining sol-free gels were measured under the same conditions resulting in the open symbols in Figure 4b (for the raw data see the Supporting Information). After extraction, $T_{2,l}$ decreased in some samples up to 50%.

Thus, the changes in mobility introduced by the gel structure are well reflected in this evaluation method especially in the shorter time constant. With increasing DC and decreasing Q_{syn}, the mobility of chains is reduced and the number of less mobile chains grows. The removal of sol decreases the mobility of mainly the mobile part.

As a second approach, the raw data can be converted to a distribution of exponential decays described by a relaxation rate $T_2^{-1} = R_2$ by using the Laplace inversion. While no additional information can be gained, a visual comparison of the data is facilitated with this approach.

dx.doi.org/10.1021/ma500558v | Macromolecules 2014, 47, 4251−4265

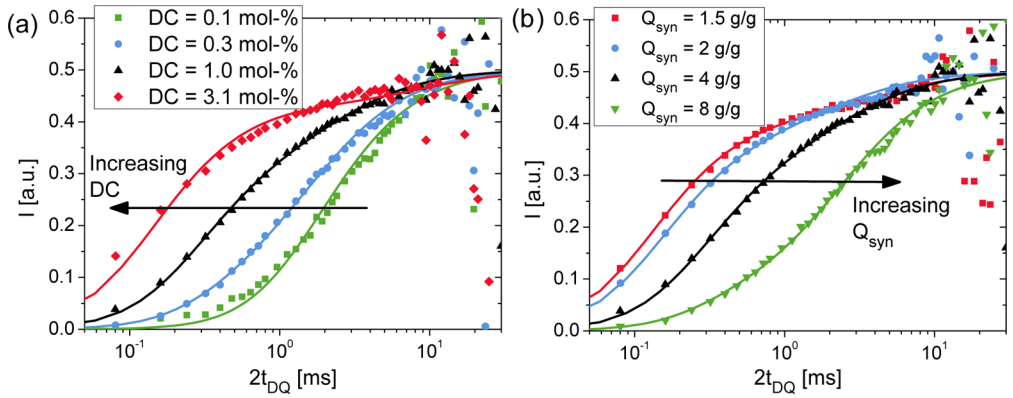

Figure 6. Double quantum coherence build-up curves of hydrogel samples are shown. The points represent the measured data as a function of the pulse sequence length t_{DQ} and the lines are bimodal fits to the data as described in the text. A series of samples with increasing degrees of cross-linking (DC) is investigated (at constant Q_{syn} = 4 g/g) in part a and the monomer concentration at the time of synthesis (Q_{syn}) is changed (at constant DC = 1 mol %) in part b.

The rate distributions are shown in Figure 5. The inversion procedure is relatively robust despite the noise in the input data and the unequal spacing of data points. The upturns observed for some samples at high T_2^{-1} values are most probably numerical artifacts.

For an increasing DC and decreasing Q_{syn}, the distributions become broader and the main peak shifts to higher relaxation rates (T_2^{-1}). In this evaluation type, the components with small relaxation rates are more easily seen and compared. All samples exhibited a tail at small rates of similar shape which was surprisingly independent of the position of the main peak. This tail is most probably the effect of the presence of residual, mobile network defects such as sol, dangling ends, and lowly cross-linked domains. All of these are more mobile when compared to the average network, however, the sol can be differentiated as it might be removed from the gel as described before.

The influence of the sol is well visible in Figure 5c. For all samples, the main effect of sol extraction was a reduction of the intensity in the mentioned small rate region. However, it also had a notable influence on the main mode of the distribution which generally shifted to higher rates (smaller time constants). Especially for the sample pAAc-DC1-Q8, a noticeable shift in the main peak was seen after extraction. This corresponded well with the high sol content measured for this sample as shown in Figure 1b. For the other samples with sol contents below 10 wt %, the changes were rather small. The extracted polymer part (sol) from the sample pAAc-DC1-Q4 was investigated separately by the same method and showed a rather slow relaxation which was described well by a single stretched exponential function yielding a time constant of 8.9 ms (not shown).

The changes revealed by removing the sol content are surprising. The sol part appears to be mobile and mainly influences the region of low rates/long relaxation times but it is partially dipolar-coupled as well and has an effect on the less mobile part. This is in contrary to previous results on (noncharged) rubbers where the sol is highly mobile if the network is sufficiently swollen.[17] Two explanations may be given for this differing behavior. One, due to the polyelectrolyte nature of the chains electrostatic interactions might reduce the mobility and induce a partially ordered rigid solution structure. Second, the presence of mobile sol chains in or close to dense parts of the network might induce a faster relaxation of the denser parts, an effect which is absent if the sol is removed.

In summary, the decay of transverse magnetization in the samples clearly reflects the differences in molecular mobility. The more the network is constrained, the faster is the magnetization decaying. However, the dynamic heterogeneity is large and, even for the most constrained networks, a highly mobile part remains. In comparison with swollen conventional rubbers, our findings indicate a substantially higher level of inhomogeneities. While the two systems seem superficially similar we could uncover distinct differences such as the very low mobile fraction of chains present in all gels no matter what the synthesis. This leads us to conclude that very dense domains exist in partly swollen gels and that they are much more inhomogeneous than swollen rubbers. The sol fraction cannot be directly identified from the relaxation behavior. The sol appears to be rather inhomogeneous as the results obtained from extracted gel samples change considerably over a large range of mobilities. The differences in mobility of the sol is probably due to branching and restricted motion inside the network matrix.

Effects of Chemical Composition on Double Quantum Coherence Build-up. The residual dipolar coupling constants (D_{res}) can be probed directly via the buildup of double- (more precisely also multiple-) quantum coherences in the cross-linked electrolyte samples. Previously, this method was mostly applied to the investigation of cured rubbers.[43,71] For the gel samples, the measurements proved challenging for two reasons. First, the noise level in the latter part of these experiments was relatively high, probably due to the relatively low polymer content in the samples and to the inhomogeneities in the magnetic field. Second, a very fast double quantum (DQ) signal build-up was found for some samples at very low DQ evolution times, which will be discussed later. As a countermeasure, the number of scans was increased and the data point spacing adjusted (see Experimental Section).

The DQ data was renormalized by fitting two exponential tails to the reference intensity. This was done in a two step process as described in earlier publications[12,72] and an example is shown in the Supporting Information. The renormalization process was in some cases ambiguous because the fitting of the exponential tails is not straightforward. This was addressed by using the same time interval for all the fits and by the fact that for long times the DQ-signal must converge to 0.5.[43] The

dx.doi.org/10.1021/ma500558v | Macromolecules 2014, 47, 4251−4265

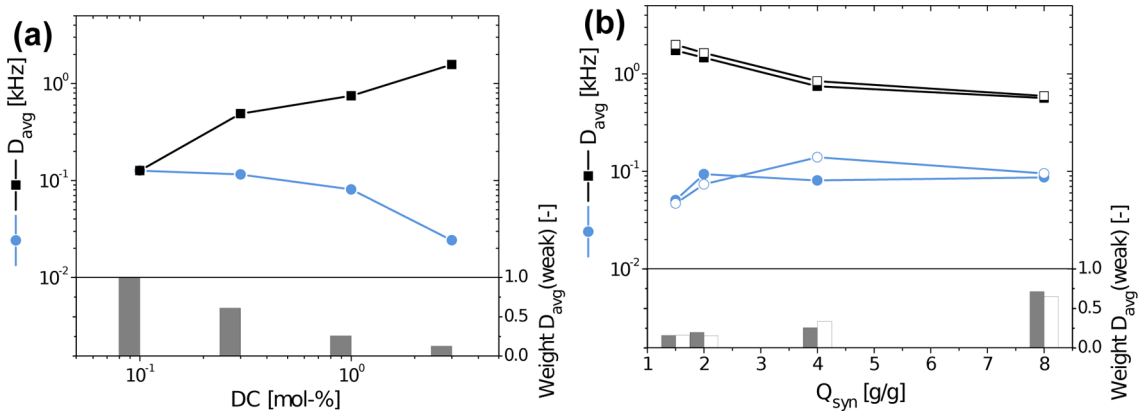

Figure 7. D_{res} fit parameters used to describe the double quantum coherence buildup of hydrogels with varying compositions are shown. The filled symbols/bars represent the as-prepared samples while the open symbols/bars in part b denote sol extracted samples. The lines are used to guide the eye while the bars give the weighting of the weak coupling constant in the bimodal fit. A series of samples with increasing degrees of cross-linking (DC) is investigated (at constant Q_{syn} = 4 g/g) in part a, and the monomer concentration at the time of synthesis (Q_{syn}) is changed (at constant DC = 1 mol %) in part b.

resulting fit constants for the exponential tails are discussed in the respective section.

The DQ coherence build-up curves of the investigated samples all had a similar form, but showed quantitative differences on the time scale of the build-up. The results are given by the symbols in Figure 6 for gels with varying values of DC and Q_{syn}. See next section for the analysis by a fit function (lines). The samples are well distinguishable but considerable scatter of the data at long DQ evolution times is observed. This is caused by the increasing signal loss over time due to relaxation effects which becomes even more pronounced after renormalization. For samples with a high DC, half of the maximum signal intensity (I = 0.25) is reached within a time that is an order of magnitude faster than for the lowest cross-linked samples. A faster build-up corresponds to a higher dipolar coupling strength and more constrained network chains. A similarly strong effect was seen for the same reasons when Q_{syn} was varied. A problem arose for the fastest signal build-up because the first data point already showed an intensity of close to 30% of the final signal. This is a clear sign of strong constraints in the sample. A faster sampling was not possible due to the rather long cycle time of the pulse sequence. This led to a noticeable inaccuracy in the measurement of the short time behavior for some samples (particularly for the sample pAAc-DC3-Q4).

While the structural differences between the samples are immediately clear in the presented data, the extraction of RDC constants and their distribution needs more advanced methods. This is achieved by the use of a Gaussian-based fit function and an inversion approach as presented in the following section.

Evaluation of Double Quantum Data. The first approach for the analysis of the data is the use of the simple fit function based on the generic Gaussian build-up function, eq 5.[73] Due to the synthesis of the hydrogels, they are composed of chains of different lengths and very different mobilities. On top of such structural inhomogeneities, the samples are characterized by substantial intrinsic swelling inhomogeneities, all leading to a broad RDC distribution. Therefore, the use of such one component build-up function, or a combination of two or three such components, is only possible in systems which are mostly free from such inhomogeneities, as is for instance the case for previously investigated noncharged model hydrogels.[12] First, a convenient and often used analytical fitting function based upon an assumed Gaussian distribution of D_{res} constants was tried (not to be mixed up with the inverse-Gaussian build-up function). This has been previously derived in ref 71 and used in the form published as eq 17 in ref 43. This did not work well, as the fitted standard deviation (width) exceeded the average, which is not physical.[71]

Another option is to rely on a numerical integration over an assumed distribution function. In this context, we have previously used a Γ function[73]

$$p(|D_{res}|) = \frac{2}{\sqrt{\pi}} \sqrt{\frac{27|D_{res}|}{8{D_{avg}}^3}}\, e^{-3|D_{res}|/(2D_{avg})} \quad (12)$$

which is bounded to positive D_{res} and has the advantage of not introducing an additional fitting parameter, as the distribution width is fixed and related to the distribution average, D_{avg}. This function was found to represent data from swollen gels and hydrogels[19,73] very well. It thus accounts well for the intrinsic swelling inhomogeneity of an otherwise homogeneously cross-linked system. Practically, the distribution integral $\int I(t_{DQ}, D_{res})\, p(|D_{res}|)\, dD_{res}$ is solved numerically by summing up over 200 discrete bins within the least-squares fitting procedure using Origin 8.1 software.

For most of the samples presented in this work, a unimodal approach using a single gamma distribution was still not a good model, indicating more pronounced inhomogeneities. Therefore, a bimodal D_{res} distribution was tested. This enabled us to satisfactorily fit all samples as shown by the lines in Figure 6. The major problem preventing a successful unimodal fit is the presence of very "rigid" parts in most samples that cannot be described by a single mode. It should to be noted that such very broad distributions are usually a conceptual challenge for the DQ normalization procedure (see the Supporting Information). The problem is that the overall intensity relaxation may be rather different for the different subcomponents,[12] invalidating the approach. In the given case, owing to the high segmental mobility, the overall relaxation is not too fast as compared to the time scale of DQ intensity build-up. A consistency check involves the measurement at different temperatures, in our case room temperature and 60 °C, and making sure that the DQ build-up behavior does not change within this temperature range.

dx.doi.org/10.1021/ma500558v | Macromolecules 2014, 47, 4251−4265

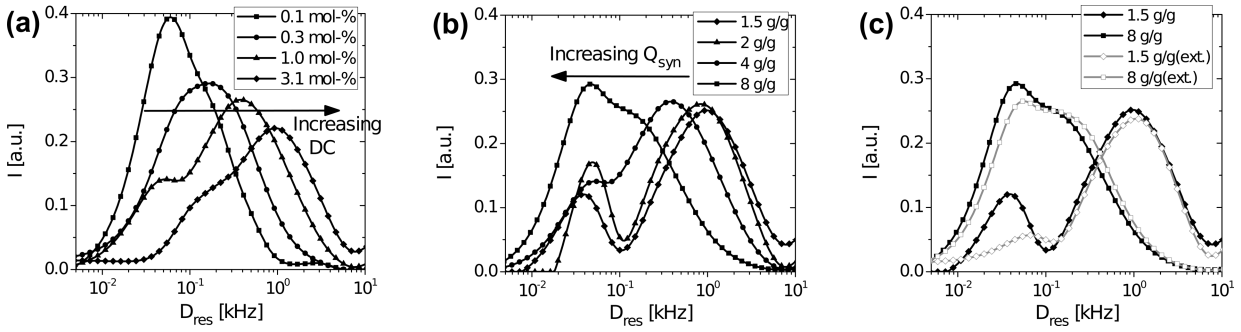

Figure 8. Distributions of the residual dipolar coupling constants (D_{res}) found in the hydrogel samples are shown. They were obtained by inversion of the DQ build-up curves shown in Figure 6 using a nonlinear regularisation method. A series of samples with increasing degrees of cross-linking (DC) was investigated (at constant Q_{syn} = 4 g/g) in part a and the monomer concentration at the time of synthesis (Q_{syn}) was changed (at constant DC = 1 mol %) in part b. The data sets with the highest and lowest Q_{syn} from part b are replotted in part c, black lines, together with the corresponding data sets where the sol has been extracted (gray lines).

From the fit, RDCs in terms of the D_{avg} constants can be extracted (see eq 5). The bimodal fit leads to two D_{avg} values, where the lower value is designated as D_{avg}(weak) and the higher one is designated as D_{avg}(strong) and also gives the respective weights of the weak coupling part. These constants are shown as a function of the gel composition in Figure 7. The difference between D_{avg}(weak) and D_{avg}(strong) constants is considerable, up to almost 2 orders of magnitude, for the most constrained samples 0.02 to 1.4 kHz for the samples pAAc-DC3-Q4. An exception is the sample pAAc-DC0.1-Q4, which did not yield a second mode. For more constrained networks (higher DC and/or lower Q_{syn}), the strongly coupled segments increase in both their coupling strength and their relative weight. This suggests an increasing amount of volume of rigid, highly confined domains. The highly constrained samples are more inhomogeneous because they still contain a small fraction of very mobile material. For the weakly coupled part, the trend is not so clear as only a small effect of the coupling strength on D_{avg}(weak) was observed. For gels still containing sol a trend to even weaker coupling for stronger constraints was observed. This effect is unexpected and the result of a small fraction of weakly coupled material that is present also on highly cross-linked samples. This might be an effect of the contained sol fraction as such low values of D_{avg}(weak) are not found for sol extracted samples (not shown).

The same measurements were conducted for the sol extracted samples where the Q_{syn} values were varied at constant DC. The results of the respective fits are also given in Figure 7 by the open symbols and bars (the DQ results of the extracted samples are given in the Supporting Information). Here, the differences in the constants as a function of Q_{syn} are mostly small when the sol-free samples are compared to the as-prepared samples. The stronger coupling constant D_{avg}(strong) was larger for all samples by 10−50% when compared to the as-prepared samples. For D_{avg}(weak) no clear trend was observed. This is an indication that the sol itself does not contribute greatly to the weak coupling part but rather influences the entire range of mobilities. It is a surprising finding that the sol does contribute to the strongly coupled part as well. It may be hypothesized that strong position and orientation correlations, generally known for polyelectrolytes, may impose strong orientational correlations on the sol chains in the denser regions.

The distributions of the D_{res} constants were obtained from the raw data by an inversion procedure based on Tikhonov regularisation. The original program was developed by Weese and modified by Chassé for use with DQ data.[48,74] The program is available online.[48] For the analysis in this work, a special ("Abragam-like") kernel function[12] was used, but a Gaussian kernel also yielded very similar results. This result can be understood as the Abragam-like function was developed to model the typical overshoot in DQ intensity often found for homogeneous networks, which is not the case for the inhomogeneous networks present in the samples. The ability to describe this overshoot is the main advantage of the new kernel function. Only raw data up to 15 ms of DQ evolution time was used, as later data points hindered effective evaluation due to high noise levels. The results of the inversion are given in Figure 8 for the series of samples.

While the distributions of the D_{res} constants were broad, the general features are somewhat clearer and less artifacts occur than in the above presented Laplace inversion results (Figure 5). In Figure 8a, the distributions shifted to higher D_{res} values as the degree of cross-linking increased. As stated above, with higher DC, a stronger coupling was found. Additionally, shoulders appeared at lower coupling constants (higher mobility) especially for samples with higher DC. This effect was previously discussed and is the reason for the occurrence and lower values of the weak coupling constants in the fits. In Figure 8b, the influence of Q_{syn} was similar except that the effect of the more mobile segments on the shoulders at lower values for D_{res} was even more pronounced. The sol extraction was able to remove a large part of the highly mobile part, but not all of it. Therefore, the main peak after extraction (gray lines in Figure 8a) shifted slightly toward stronger coupling.

When compared to conventional swollen rubber samples investigated at similar DC and swelling, the measured D_{res} distributions are, as mentioned, very broad.[48] Charged hydrogels contain very strongly coupled segments leading to a very fast initial build-up that is not usually present in rubbers. Additionally, the final DQ intensity is reached much more quickly in most rubbers relative to these gel samples. As a result, the overshoot in the DQ-build-up that arises for quantum-mechanical reasons and is often observed in rubbers, and that can be fitted and accounted for by the mentioned empirical build-up function,[48] is not observed in charged gels as it is smeared out due to network heterogeneity. Hence, the Gaussian-shaped basis function is suitable to describe the DQ build-up for the samples investigated herein.

dx.doi.org/10.1021/ma500558v | Macromolecules 2014, 47, 4251−4265

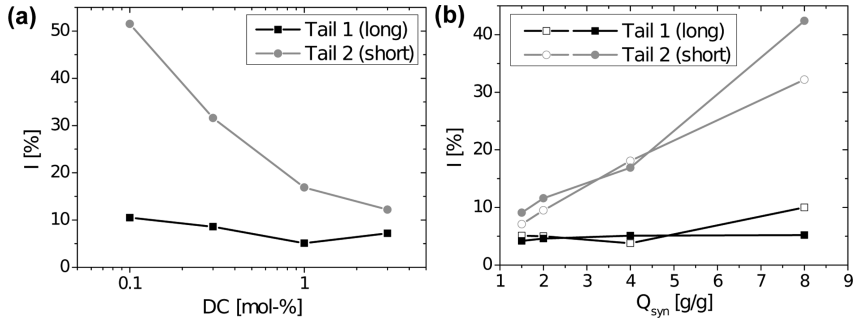

Figure 9. Weights of the two exponential components subtracted in the evaluation of double quantum build-up data are shown. The exact evaluation procedure is described in the Supporting Information and in refs 12 and 72. A series of samples with increasing degrees of cross-linking (DC) is investigated (at constant Q_{syn} = 4 g/g) in part a, and the monomer concentration at the time of synthesis (Q_{syn}) is changed (at constant DC = 1 mol %) in part b. The solid symbols represent the as-prepared samples while the open symbols in part b denote sol extracted samples.

In summary, the DQ method is able to clearly differentiate between the investigated samples. The build-up in DQ intensity is faster for less mobile polymer chains (high DC, low Q_{syn}). The corresponding residual dipolar coupling constants (D_{res}) can be extracted by fit functions based on a Gaussian kernel or by an inversion procedure with a specialized kernel function. This is especially useful to investigate the development of mobile parts in more constrained samples or the influence of sol extraction.

Analysis of Components Obtained by the DQ and T_2 Methods. The weights of components and modes were obtained by three different fit approaches and can be compared to each other. These methods are the fit of transverse relaxation data as given by Figure 4 (two polymer components and HDO), the fit of DQ build-up data given in Figure 7 (bimodal), and the above-mentioned two exponential tails obtained in the evaluation of the DQ data. The latter approach yields two components, and their weights are given in Figure 9 for the variation of DC and Q_{syn}, respectively. As both methods ultimately probe the same phenomena, these two components should be comparable to the long-time components extracted from the transverse relaxation data.

The exponential component with the long time constant fitted to the DQ data has a low weight between 5−10% and a time constant is the order of 200 ms for all samples. Both constants are not a function of the material. The signal is probably rising due to residual HDO which is also measured by the longest T_2 in the transverse relaxation method. In the latter case, time constants of several seconds and weights in the order of 40% are found, independently of the material as well. The quantitative differences are a result of different recycle delays. The short recycle delay of 0.1 s for DQ acts as filter for the slowly relaxing HDO which is fully recovered in the 20 s used for CPMG.

The exponential component in the DQ data with the shorter time constant is related to the polymer. The time constant is on the order of 10 ms and does not depend on the gel composition while the weight increases strongly with with less constraints in the network (higher Q_{syn} and lower DC). Upon extraction, both, time constant and weight, are lowered by 20−30% except for the sample pAAc-DC1-Q4. This is similar to the time constant $T_{2,l}$ from the decay of transverse magnetization which is in the order of 20 ms independent of the gel and its weight increases in the same direction. However, for $T_{2,l}$ the weight is lower so it probably does not reflect exactly the same component. These facts point to the conclusion that this component is composed of mobile defects as discussed in previous works. One part is sol as can be proven by the reduction upon extraction. The variation in the weight supports this as mobile defects are likely to increase at lower DC and higher Q_{syn}. Qualitatively, the trend is similar found to the one in the sol content shown in Figure 1 but the sol part is much lower.

The fast relaxing component from the transverse relaxation data ($T_{2,s}$) corresponds to the two modes identified in the DQ build-up curves. These components relate to the gel structure. In this case, the resolution from the DQ method is better as two different modes are easily identified as opposed to the single mode in the transverse relaxation data.

Comparison with Industrial Samples. In this last part, all previously evaluated methods are applied to samples of commercial origin to demonstrate their relevance to real world applications. Two commercial samples are investigated here, both composed of cross-linked poly(acrylic acid). The gel designated L1030 is homogeneously cross-linked, while the LB1110 gel features the additional surface cross-links typically found for superabsorbers used in diaper products. Unfortunately, the cross-link densities are unknown but the proposed experiments can be used to estimate them (see below). The transverse relaxation curves are shown in Figure 10 and include results from our sample pAAc-DC1-Q4 for comparison.

The two commercial samples show distinctly different relaxation behavior. For the sample LB1110, a fast decay is first observed, however, a very slowly decaying component is also present. In contrast, the sample L1030 decays generally

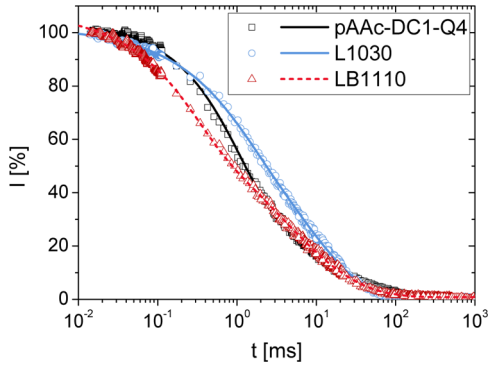

Figure 10. Transverse magnetization decay for commercial hydrogels is compared to a self-synthesized sample (DC = 1 mol %, Q_{syn} = 4 g/g). The raw data (symbols) is shown with the respective fits of eq 11 (lines). The obtained time constants are given in the text.

dx.doi.org/10.1021/ma500558v | Macromolecules 2014, 47, 4251−4265

slower. The decay behavior of the self-synthesized gel is on a comparable time-scale but is broader. It decays slower than the fast part of LB1110 but is similar to its slow part. This may be quantified using the fit function eq 11. The fast relaxing component has a weight of 45% and $T_{2,s}$ = 0.41 ms for LB1110 compared to $T_{2,s}$ = 1.0 ms and 22% for L1030. The slow relaxing component shows a similar behavior for both gels with $T_{2,l}$ = 8.6 ms (LB1110) to 7.5 ms (L1030) and a stretching exponent of about 0.6 in both cases. While the separation between the two fitted T_2 constants is largest for LB1110 the core−shell structure is not reflected in the width of the slower mode.

The differences between the three samples become even clearer when applying the DQ method. Figure 11 shows a

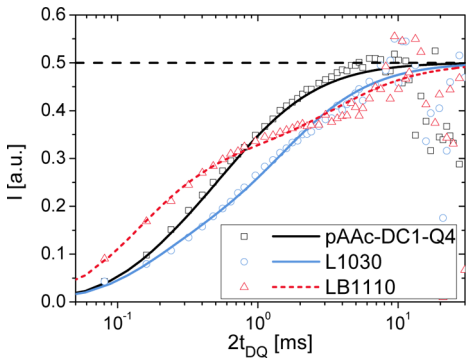

Figure 11. Double quantum coherence build-up curves for commercial hydrogel samples are compared to a self-synthesized sample (DC = 1 mol %, Q_{syn} = 4 g/g). The points represent the measured data as a function of the pulse sequence length t_{DQ} and the lines are bimodal fits to the data as described in the Experimental Section.

much slower build-up for the homogeneous sample L1030, a faster build-up for pAAc-DC1-Q4 and the LB1110 gel exhibits a clear bimodal build-up composed of a very fast and a slow component. The two-component fits are shown as well leading to values for the average coupling equal to D_{avg}(weak) = 0.1 and D_{avg}(strong) = 1.6 kHz for LB1110 and D_{avg}(weak) = 0.15 and D_{avg}(strong) = 1.2 kHz for L1030. The bimodal behavior of LB1110 is clearly seen in the build-up curves and also in the large difference between the D_{res} constants.

The same conclusions can be drawn by just looking at the distributions obtained from inverse methods as shown in Figure 12. Already, in the Laplace inversion data (a), the distribution of inverse T_2 for LB1110 is quite broad and features a clear bimodal behavior while the data for L1030 is shifted to lower relaxation rates, is slightly less broad. After the Tikhonov regularisation (b), the bimodality of the LB1110 sample as opposed to L1030 or the self-synthesized samples is even clearer. The two modes in LB1110 are baseline separated while the other samples feature a continuous distribution and show shoulders. By comparison of the distributions of the commercial samples with the samples in Figure 8, an approximate value for DC can be estimated. For L1030, DC is estimated to be in the range of 0.3 mol % and, for LB1110, the DC of the two domains is on the order of 0.1 and 3 mol % with a ratio of about 1:2.

Therefore, the methods to quantify the mobility in hydrogels developed for model gels can also be applied with considerable success to commercial samples. These samples contain less sol and L1030 is slightly less heterogeneous than the self-synthesized samples. This makes the data acquisition and evaluation easier. While all methods can distinguish between the domains for samples with two domains, the difference is clearest in the distribution of RDCs obtained by Tikhonov regularization.

CONCLUSIONS

In the present study, we explored the dynamics in poly(acrylic acid) hydrogels by low-field ^{1}H NMR methods. Two experimental methods allowed for quantifying the strength of residual dipolar coupling (RDC) in these constrained systems. The RDCs characterize the cross-link-induced chain motion anisotropy and are proportional to a dynamic order parameter which depends on the inverse mesh size at constant degree of swelling. The measurement of the transverse magnetization decay and the buildup of the double quantum coherences provided insight into the local mobility of the network. The latter method was applied for the first time to this type of system. The mobility was successfully correlated with topological constraints controlled by varying the synthesis conditions. However, both NMR methods needed to be adapted to charged gels to obtain the results presented here. Specifically, the pulsed spin-locking effect must be prevented in networks where the longitudinal relaxation in the rotating frame occurs on a similar time scale as the transverse relaxation. This important adverse effect is not limited to hydrogels but should be relevant for any study of samples with substantial RDCs.

It was shown that all gel samples exhibited a very broad distribution of order parameters, thus effective mesh sizes. The

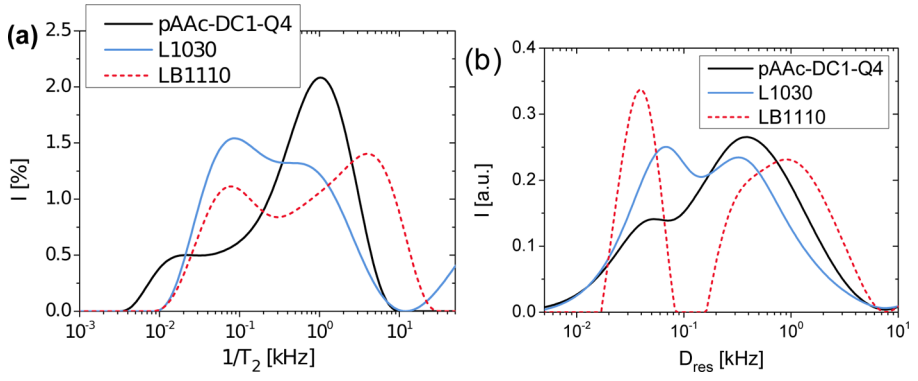

Figure 12. Distributions of inverse T_2 time constants (a) is compared the D_{res} distributions (b) for commercial hydrogel samples. The results are compared to a previously shown self-synthesized sample (DC = 1 mol %, Q_{syn} = 4 g/g). The distributions were obtained from the data shown above.

dx.doi.org/10.1021/ma500558v | Macromolecules 2014, 47, 4251−4265

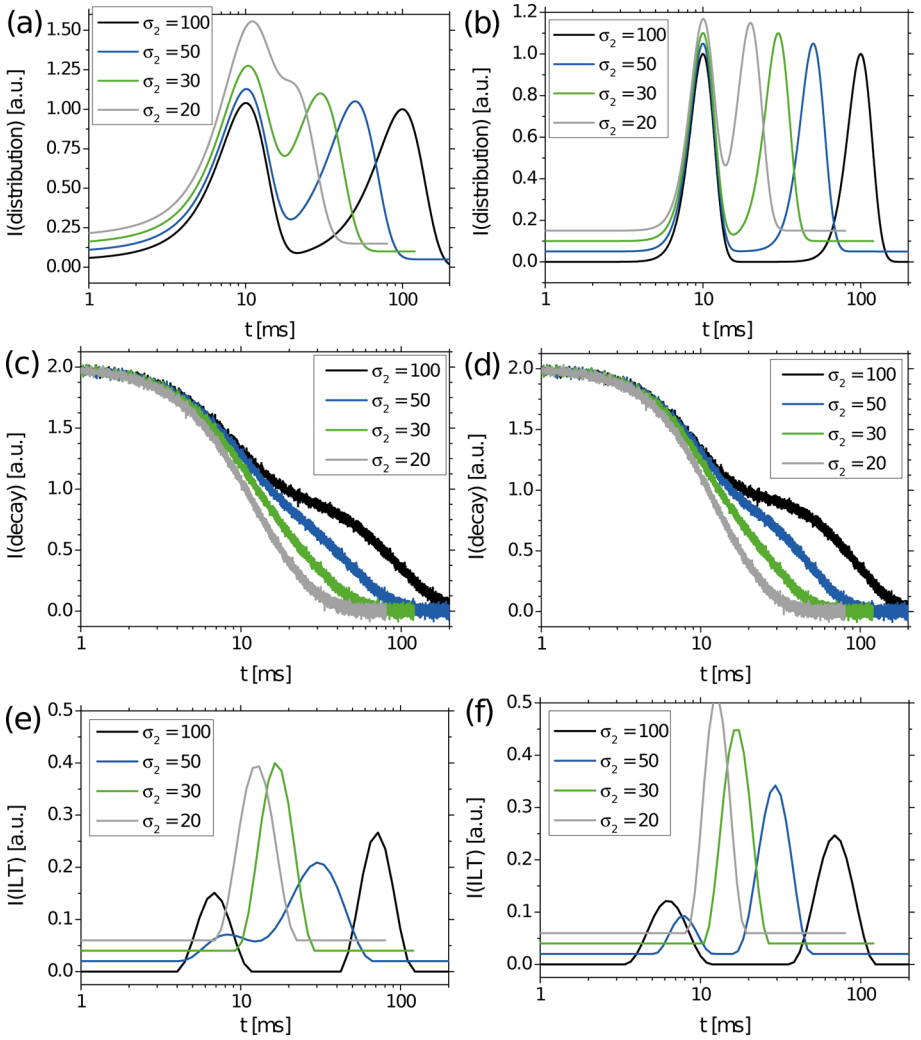

Figure 13. Synthetic data is generated from bimodal Gaussian distributions of Gaussian functions (a and b) by a variation of the mode's width and the center of the second mode. The data sets are plotted with an offset of 5% each for better visibility. The corresponding signal decay is calculated and noise added (c and d) and the data sets treated by Laplace inversion (e and f). Eight examples are shown here. The position of the second mode (σ_2) is varied with respect to the first in four steps as indicated by the caption. Additionally, cases of narrow (b, d, f) and broad peaks are compared (a, c, e). For details and interpretation, see the text.

distribution of T_2 relaxation times and RDCs spanned 2−3 orders of magnitude in time respectively frequency, respectively, and were composed of very rigid to highly mobile chains. This poses a problem for data acquisition and visualization methods alike. The underlying heterogeneity is best visible as a distribution by the use of an inversion method to display the probability distribution of inverse T_2 times or RDCs, respectively. This can potentially be a first step in obtaining real mesh size distributions of networks, provided the swelling-induced and intrinsic inhomogeneous changes in topology and the distribution of local strain can be contained or understood better.

By varying the synthesis, model gels with large differences in the dynamics and properties were obtained. By decreasing the degree of cross-linking or increasing the water content during synthesis, the equilibrium swelling capacity as well as the sol content increased and topological constraints in the samples were reduced. This was universally reflected in a slower transverse relaxation and a slower double quantum coherence build-up. The differences were well resolved and a clear effect was found. The investigation of the sol-extracted samples showed that the sol was not a homogeneous component. It is made up of rather mobile chains but also contains less mobile parts. The sol is a priori indistinguishable from the rest of the network. Therefore, the assignment of relaxation components to a specific fraction seems ambiguous for the samples investigated here. An illustrative representation of the dynamic differences was achieved by inverse transformation methods.

In principle, the two NMR methods were able to obtain similar information for the hydrogel samples. As an advantage the transverse relaxation method is often already implemented on the spectrometers in use but quantitatively better results are obtained with the double quantum method. Nevertheless, despite the conceptual shortcomings, our study shows that the gel inhomogeneity, in particular the rough amount and relative mobility of rather distinct network components and the overall distribution width, is well reflected in the data. The double-quantum method has the advantage that the distribution RDC constants can be extracted without ambiguities related to the time scale of motion and the unknown shape of the relaxation function (which does systematically affect the obtained T_2 distributions). The DQ method is therefore suggested for

dx.doi.org/10.1021/ma500558v | *Macromolecules* 2014, 47, 4251−4265

quantitative studies. These more quantitative results do resemble the relaxation rate distributions and thus provide a validation. It remains to be investigated in how far the more quantitative results from the DQ method may be useful for selectively establishing structure−property relationships.

Polyelectrolyte hydrogel samples of commercial origin are successfully investigated by the same methods. These samples have a better defined structure, but still feature significant inhomogeneity. By comparison, the approximate degree of cross-linking and the fractions of the well-distinguishable components in these samples can be estimated. For a sample with additional surface cross-linking, the bimodal structure was clearly recovered by both methods, but more selectively by the double-quantum method.

To extend the current study it seems worthwhile to vary the gel dynamics not only through changes in the structure but also by the addition of an electrolyte. This would reduce the chain stiffness via its influence on the electrostatic persistence length and render the chains more mobile when more ions are present. The exploration of this phenomenon will likely contribute to a better understanding of electrostatic repulsion and screening effects in polyelectrolyte networks.

APPENDIX: TEST OF ILT WITH ARTIFICIAL GAUSSIAN DATA

The inverse Laplace transform (ILT) is mathematically only suitable for the inversion of data sets composed of exponential decays. Due to this theoretical constraint, objections are often raised as to the application to transverse magnetization decays, as they are likely to contain Gaussian components. This conflict can be illustrated by the fact that close to time zero the Gauss function has a zero derivative in contrast to the exponential function.

Here, we use synthetic data to test if decays containing Gaussian decays may nevertheless be analyzed using the ILT technique. The data is constructed from bimodal distributions of Gaussian decays (200 functions each). The modes were itself Gaussian shaped with the center of the modes being 10 ms for the first mode and 100, 50, 30, and 20 ms for the second mode. The width of the modes was 25% (narrow case) or 50% (broad case) of the respective center value. The centers of the 200 Gaussian functions are evenly distributed over the modes width. This leads to eight cases of two mode distributions as shown in Figure 13, parts a and b, for broad and narrow cases, respectively. Each distribution was converted to a decay by assigning each individual Gaussian function the weight as given by the enveloping mode. The decay data for each mode was normalized separately to one, both are added up and noise is added to the data sets (Figure 13, parts c and d). The synthetic decay data is fed into the ILT routine as described above. The resulting decay time distributions are given by Figure 13, parts e and f.

When comparing the original distributions to the ones obtained after ILT qualitative similarities are seen. If the two original modes are well separated, they are well distinguishable after the ILT as well. The differences in the peak's location can be attributed to the $1/\sqrt{2}$ prefactor of a Gaussian when compared to an exponential function. The width of the modes is about 40% of the center value for all peaks no matter if the narrow or broad cases are investigated. This seems to be an artifact of the smoothing parameter used in the ILT procedure which has a strong influence on the peak width and was similar in all cases. If the original modes are closely spaced (σ_2 = 20 or 30 ms) the modes cannot be distinguished after inversion and only a single peak is observed. It can therefore be concluded that at least in this model case the ILT on Gaussian data provides qualitatively correct results in the sense that the peak centers are approximately correct. The distribution's width needs, however, to be treated with caution as they are very sensitive to the smoothing parameter. We suggest that not all applications of ILT on (partly) Gaussian decays have to be dismissed a priori but the results should be considered with care.

ASSOCIATED CONTENT

Supporting Information

Phase cycles for CPMG, XX4, and XY16 -pulse trains, description of the procedure for the treatment of transverse relaxation data, transverse relaxation data of sol extracted hydrogels (Figure S1), full list of constants of the fitting of transverse relaxation data, description of the procedure for the treatment of double quantum build-up data, and double quantum build-up data of sol extracted samples. This material is available free of charge via the Internet at http://pubs.acs.org.

AUTHOR INFORMATION

Corresponding Authors

*(K.S.) E-mail: kay.saalwaechter@physik.uni-halle.de.
*(M.W.) E-mail: manfred.wilhelm@kit.edu.

Notes

The authors declare no competing financial interest.

ACKNOWLEDGMENTS

The authors are indebted to P. Galvosas (University of Wellington) for access to the Inverse Laplace transform (ILT) implementation. J.H. acknowledges funding from the DFG priority program 1259 "Smart hydrogels" and the Heinrich Böll Stiftung. G.G. thanks the DFG for financial support (priority program 1369 and Pro^{2}NMR). J.H. would like to thank Karl Ratzsch (KIT) for maintaining the NMR-instrument and helpful discussions as well as Karin Schlag (KIT) for the preparation of some samples. The authors thank Jennifer Kübel (KIT) for help during the preparation of this manuscript.

REFERENCES

(1) de las Heras Alarcon, C.; Pennadam, S.; Alexander, C. *Chem. Soc. Rev.* **2005**, *34*, 276.
(2) Zhao, Y.-L.; Stoddart, J. F. *Langmuir* **2009**, *25*, 8442.
(3) Sun, J.-Y.; Zhao, X.; Illeperuma, W. R. K.; Chaudhuri, O.; Oh, K. H.; Mooney, D. J.; Vlassak, J. J.; Suo, Z. *Nature* **2012**, *489*, 133.
(4) Tuncaboylu, D. C.; Sahin, M.; Argun, A.; Oppermann, W.; Okay, O. *Macromolecules* **2012**, *45*, 1991.
(5) Qiu, Y.; Park, K. *Adv. Drug Delivery Rev.* **2012**, *64*, 49.
(6) *Hydrogel Sensors and Actuators—Engineering and Technology*, 1st ed.; Gerlach, G., Arndt, K.-F., Eds.; Springer: Berlin, 2010.
(7) Höpfner, J.; Klein, C.; Wilhelm, M. *Macromol. Rapid Commun.* **2010**, *31*, 1337.
(8) Höpfner, J.; Richter, T.; Košovan, P.; Holm, C.; Wilhelm, M. *Prog. Colloid Polym. Sci.* **2013**, *140*, 117.
(9) Höpfner, J. *A new method of seawater desalination via acrylic acid based hydrogels: Synthesis, characterisation, and experimental realisation*, 1st ed.; KIT Scientific Publishing: Karlsruhe, Germany, 2013.
(10) Flory, P. J. *Principles of Polymer Chemistry*, 1st ed.; Cornell University Press: Ithaca, NY, 1953.

(11) Sakai, T.; Matsunaga, T.; Yamamoto, Y.; Ito, C.; Yoshida, R.; Suzuki, S.; Sasaki, N.; Shibayama, M.; Chung, U.-i. *Macromolecules* **2008**, *41*, 5379.
(12) Lange, F.; Schwenke, K.; Kurakazu, M.; Akagi, Y.; Chung, U.; Lang, M.; Sommer, J.-U.; Sakai, T.; Saalwaechter, K. *Macromolecules* **2011**, *44*, 9666.
(13) Queslel, J. P.; Mark, J. E. *J. Chem. Phys.* **1985**, *82*, 3449.
(14) Mendes, J. E.; Lindner, P.; Buzier, M.; Boué, F.; Bastide, J. *Phys. Rev. Lett.* **1991**, *66*, 1595.
(15) Schosseler, F.; Ilmain, F.; Candau, S. J. *Macromolecules* **1991**, *24*, 225.
(16) Shapiro, Y. E. *Prog. Polym. Sci.* **2011**, *36*, 1184.
(17) Chassé, W.; Schlögl, S.; Riess, G.; Saalwächter, K. *Soft Matter* **2013**, *9*, 6943.
(18) Saalwächter, K.; Kleinschmidt, F.; Sommer, J.-U. *Macromolecules* **2004**, *37*, 8556.
(19) Valentín, J. L.; López, D.; Hernández, R.; Mijangos, C.; Saalwächter, K. *Macromolecules* **2009**, *42*, 263.
(20) Chassé, W.; Saalwächter, K.; Sommer, J.-U. *Macromolecules* **2012**, *45*, 5513.
(21) Blümler, P.; Blümich, B. *Rubber Chem. Technol.* **1997**, *70*, 468.
(22) Schneider, M.; Demco, D.; Blümich, B. *J. Magn. Reson.* **1999**, *140*, 432.
(23) Schneider, M.; Gasper, L.; Demco, D. E.; Blümich, B. *J. Chem. Phys.* **1999**, *111*, 402.
(24) Litvinov, V. M.; Orza, R. A.; Klüppel, M.; van Duin, M.; Magusin, P. C. M. M. *Macromolecules* **2011**, *44*, 4887.
(25) Litvinov, V. M. *Macromolecules* **2001**, *34*, 8468.
(26) Adriaensens, P.; Storme, L.; Carleer, R.; D'Hae, J.; Gelan, J.; Litvinov, V. M.; Marissen, R.; Crevecoeur, J. *Macromolecules* **2001**, *35*, 135.
(27) Kimmich, R. *NMR: Tomography, Diffusiometry, Relaxometry*, 1st ed.; Springer: Berlin, 1997.
(28) Addad, J. P. C. In *Spectroscopy of Rubbers and Rubbery Materials*, 1st ed.; Litvinov, V. M., De, P. P., Eds.; RAPRA Technology Ltd.: Shawbury, U.K., 2002; p 291.
(29) Litvinov, V. M.; Dias, A. A. *Macromolecules* **2001**, *34*, 4051.
(30) Litvinov, V. M.; Steeman, P. A. M. *Macromolecules* **1999**, *32*, 8476.
(31) Klüppel, M.; Menge, H.; Schmidt, H.; Schneider, H.; Schuster, R. H. *Macromolecules* **2001**, *34*, 8107.
(32) Litvinov, V. M.; Barendswaard, W.; van Duin, M. *Rubber Chem. Technol.* **1998**, *71*, 105.
(33) Cohen-Addad, J.; Domard, M.; Lorentz, G.; Herz, J. *J. Phys. (Paris)* **1984**, *45*, 575.
(34) Valentín, J. L.; Posadas, P.; Ferández-Torres, A.; Malmierca, M. A.; González, L.; Chassé, W.; Saalwächter, K. *Macromolecules* **2010**, *43*, 4210.
(35) Hills, B. P.; Cano, C.; Belton, P. S. *Macromolecules* **1991**, *24*, 2944.
(36) Tomić, K.; Veeman, W. S.; Boerakker, M.; Litvinov, V. M.; Dias, A. A. *J. Pharm. Sci.* **2008**, *97*, 3245.
(37) Di Lorenzo, F.; Seiffert, S. *Macromolecules* **2013**, *46*, 1962.
(38) Klüppel, M. *Prog. Colloid Polym. Sci.* **1992**, *90*, 137.
(39) Hölzl, T.; Trautenberg, H. L.; Göritz, D. *Phys. Rev. Lett.* **1997**, *79*, 2293.
(40) Bain, A. D.; Eaton, D. R.; Hamielec, A. E.; Mlekuz, M.; Sayer, B. G. *Macromolecules* **1989**, *22*, 3561.
(41) Mellinger, F.; Wilhelm, M.; Belik, P.; Schwind, H.; Spiess, H. W. *Macromol. Chem. Phys.* **1999**, *200*, 2454.
(42) Dalitz, F.; Cudaj, M.; Maiwald, M.; Guthausen, G. *Prog. Nucl. Magn. Reson. Spectrosc.* **2012**, *60*, 52.
(43) Saalwächter, K. *Prog. Nucl. Magn. Reson. Spectrosc.* **2007**, *51*, 1.
(44) Bloembergen, N.; Purcell, E. M.; Pound, R. V. *Phys. Rev.* **1948**, *73*, 679.
(45) Slichter, C. P. *Principles of Magnetic Resonance*, 2nd ed.; Springer-Verlag: New York, 1978.
(46) Saalwächter, K. *Macromolecules* **2005**, *38*, 1508.
(47) Graf, R.; Demco, D. E.; Hafner, S.; Spiess, H. W. *Solid State Nucl. Magn. Reson.* **1998**, *12*, 139.
(48) Chassé, W.; Valentín, J. L.; Genesky, G. D.; Cohen, C.; Saalwächter, K. *J. Chem. Phys.* **2011**, *134*, 44907.
(49) Kanekiyo, M.; Kobayashi, M.; Ando, I.; Kurosu, H.; Ishii, T.; Amiya, S. *J. Mol. Struct.* **1998**, *447*, 49.
(50) Hong, P.-D.; Chen, J.-H. *Polymer* **1998**, *39*, 5809.
(51) Callaghan, P.; Godefroy, S.; Ryland, B. *J. Magn. Reson.* **2003**, *162*, 320.
(52) Callaghan, P.; Godefroy, S.; Ryland, B. *Magn. Reson. Imaging* **2003**, *21*, 243.
(53) Widder, D. V. *Am. Math. Mon.* **1945**, *52*, 419.
(54) Honerkamp, J. *Stochastic dynamical systems: concepts, numerical methods, data analysis*, 1st ed.; VCH: New York, 1994.
(55) Oppermann, W. Swelling Behavior and Elastic Properties of Ionic Hydrogels. In *Polyelectrolyte Gels - Properties, Preparation, and Applications*, 1st ed.; Harland, R. S., Prud'homme, R. K., Eds.; American Chemical Society: Washington DC, 1992; p 159.
(56) Umendra, D.; Metha, S. K.; Choudhary, M. S.; Jain, R. *Rev. Macromol. Chem. Phys.* **1999**, *C39*, 507.
(57) Vervoort, S.; Patlazhan, S.; Weyts, J.; Budtova, T. *Polymer* **2005**, *46*, 121.
(58) Buchholz, F. L.; Graham, A. T. *Modern Superabsorbent Polymer Technology*, 1st ed.; Wiley-VCH: New York, 1998.
(59) Pines, A.; Rhim, W.-K.; Waugh, J. S. *J. Magn. Reson.* **1972**, *6*, 457.
(60) Maus, A.; Hertlein, C.; Saalwächter, K. *Macromol. Chem. Phys.* **2006**, *207*, 1150.
(61) Carr, H.; Purcell, E. *Phys. Rev.* **1954**, *94*, 630.
(62) Meiboom, S.; Gill, D. *Rev. Sci. Instrum.* **1958**, *29*, 688.
(63) Hahn, E. L. *Phys. Rev.* **1950**, *80*, 580.
(64) Gullion, T.; Baker, D. B.; Conradi, M. *J. Magn. Reson.* **1990**, *89*, 479.
(65) Hoult, D. I.; Richards, R. E. *Proc. R. Soc. London, A: Math. Phys.* **1975**, *344*, 311.
(66) Liu, Y.; Chan-Park, M. B. *Biomaterials* **2009**, *30*, 196.
(67) Wack, H.; Ulbricht, M. *Polymer* **2009**, *50*, 2075.
(68) Ostroff, E. D.; Waugh, J. S. *Phys. Rev. Lett.* **1966**, *16*, 1097.
(69) Guthausen, A.; Zimmer, G.; Blümler, P.; Blümich, B. *J. Magn. Reson.* **1998**, *130*, 1.
(70) Shaka, A. J.; Rucker, S. P.; Pines, A. *J. Magn. Reson.* **1988**, *77*, 606.
(71) Saalwächter, K.; Ziegler, P.; Spyckerelle, O.; Haidar, B.; Vidal, A.; Sommer, J.-U. *J. Chem. Phys.* **2003**, *119*, 3468.
(72) Saalwächter, K. *Rubber Chem. Technol.* **2012**, *85*, 350.
(73) Saalwächter, K.; Sommer, J.-U. *Macromol. Rapid Commun.* **2007**, *28*, 1455.
(74) Weese, J. *Comput. Phys. Commun.* **1992**, *69*, 99.